

Particle Acceleration at Relativistic Shocks

Yves A. Gallant^{1,2}

¹ Osservatorio Astrofisico di Arcetri, Largo E. Fermi 5, 50125 Firenze, Italy

² Astronomical Institute Utrecht, Postbus 80 000, 3508 TA Utrecht, Netherlands

Abstract. I review the current status of Fermi acceleration theory at relativistic shocks. I first discuss the relativistic shock jump conditions, then describe the non-relativistic Fermi mechanism and the differences introduced by relativistic flows. I present numerical calculations of the accelerated particle spectrum, and examine the maximum energy attainable by this process. I briefly consider the minimum energy for Fermi acceleration, and a possible electron pre-acceleration mechanism.

1 Introduction and Motivation

A ubiquitous feature of astrophysical objects involving relativistic flows, such as active galactic nuclei (AGNs), gamma-ray bursts (GRBs) and Crab-like supernova remnants (SNRs), is the presence of nonthermal, power-law emission spectra (i.e. with flux density $F_\nu \propto \nu^{-\alpha}$, where ν is the frequency and α the spectral index), in particular in the radio and hard X-ray or gamma-ray domains. This emission is believed to be produced by accelerated particles having a corresponding power-law energy spectrum; more specifically, in most of these objects the emission is thought to be from accelerated electrons radiating via the synchrotron or inverse Compton mechanisms (see Mastichiadis, this volume). The aim of the present review will be to discuss the probable mechanism of this acceleration and the spectra that may be expected theoretically.

The most widely invoked mechanism for the acceleration of particles to power-law spectra in non-relativistic contexts, such as SNR blast waves or interplanetary shocks, is *Fermi acceleration*. It seems likely that shocks are responsible for particle acceleration in relativistic flows as well, and this is indeed explicitly assumed in models of GRBs and Crab-like SNRs. It is then natural to consider how the Fermi mechanism could operate at relativistic shocks, and what the resulting spectrum would be. The focus of this contribution will thus be the relativistic version of Fermi shock acceleration.

This review is organised as follows: in Sect. 2, I discuss the shock jump conditions at relativistic shocks, emphasising the aspects relevant to particle acceleration; this section is intended to be self-contained. In Sect. 3, I describe the Fermi acceleration mechanism in detail, first reviewing its main features in the context of non-relativistic shocks, and then presenting the resulting spectrum for ultra-relativistic and more moderately relativistic shocks. In Sect. 4, I examine the acceleration time scale and the maximum energy attainable by this mechanism, and consider the minimum energy for Fermi acceleration of electrons in an electron-ion shock, and a possible pre-acceleration mechanism.

2 Relativistic Shocks

The properties of shocks most important for Fermi-type particle acceleration are the velocities of the shock relative to the upstream and downstream frames. These are obtained through the *shock jump conditions*.

2.1 Relativistic Shock Jump Conditions

The shock jump conditions are derived from the laws of conservation of particle number, energy, and momentum. For relativistic fluids, these are, in order:

$$\Gamma_1 \beta_1 n_1 = \Gamma_2 \beta_2 n_2, \quad (1)$$

$$\Gamma_1^2 \beta_1 (\varepsilon_1 + p_1) = \Gamma_2^2 \beta_2 (\varepsilon_2 + p_2), \quad (2)$$

$$\Gamma_1^2 \beta_1^2 (\varepsilon_1 + p_1) + p_1 = \Gamma_2^2 \beta_2^2 (\varepsilon_2 + p_2) + p_2, \quad (3)$$

where subscripts 1 and 2 respectively refer to the upstream and downstream regions, n , ε and p are the fluid number density, energy density and pressure, all measured in the local fluid rest frame, β is the fluid velocity in units of the speed of light c , and Γ the corresponding Lorentz factor. The fluid velocities are measured in the *shock frame*, where the shock is stationary and both velocity vectors lie along the shock normal. Equivalently, β_1 and β_2 may be viewed as the shock velocity with respect to the upstream and downstream fluids.

For simplicity, I restrict my attention in this review to unmagnetised shocks. The shock jump conditions for relativistic magneto-hydrodynamics (MHD) were reviewed by Kirk and Duffy [20]. They can yield shock jump conditions which differ significantly from those derived here when the magnetisation parameter,

$$\sigma \equiv \frac{B_1^2}{4\pi(\varepsilon_1 + p_1)}, \quad (4)$$

where B is the magnetic field measured in the local fluid rest frame, is not negligibly smaller than unity [19,21].

2.2 Ultra-Relativistic Shocks

Much of the discussion of particle acceleration below will be specialised to ultra-relativistic shocks, i.e. those in which the shock Lorentz factor $\Gamma_{\text{sh}} \equiv \Gamma_1 \gg 1$, and $\beta_1 \approx 1$. In that case the pressure term p_1 may be neglected in (3) relative to the first term. The particles downstream of such a shock must be heated to highly relativistic temperatures; assuming they obey the ultra-relativistic gas equation of state, $\varepsilon_2 = 3p_2$, one may then solve (2) and (3) to obtain the *ultra-relativistic shock jump conditions*, yielding the downstream velocity

$$\beta_2 \approx \frac{1}{3}. \quad (5)$$

Also of interest is the relative velocity β_{rel} of the upstream and downstream fluids. Using the relativistic velocity addition formula,

$$\beta_{\text{rel}} = \frac{\beta_1 - \beta_2}{1 - \beta_1\beta_2}, \quad (6)$$

the associated Lorentz factor in the ultra-relativistic limit is $\Gamma_{\text{rel}} \approx \Gamma_{\text{sh}}/\sqrt{2}$.

It should be noted that these shock jump conditions are independent of the upstream equation of state, and depend only on the downstream gas being ultra-relativistically hot. It will be seen below that particle acceleration in the ultra-relativistic shock regime thus mirrors some of the simplicity of the non-relativistic, strong shock regime, due to the existence of this single, well-defined asymptotic value (for weakly magnetised shocks) of the shock velocity ratio.

2.3 Moderately Relativistic Shocks

For more general values of the shock Lorentz factor Γ_{sh} , the shock jump conditions depend on the equation of state and the temperature of the upstream gas. For illustration, the two opposite extremes of an ultra-relativistically hot and a cold gas upstream will be examined.

Shocks in an Ultra-Relativistic Gas

I first assume that the gas upstream of the shock already has a highly relativistic temperature; this might be the case for an internal shock in a GRB fireball, for instance, if it propagates in a medium already heated by previous shell collisions (see e.g. Sari & Galama, this volume). In this case, both the upstream and the downstream media can be assumed to follow the ultra-relativistic equation of state, $\varepsilon = 3p$. Equations (2) and (3) are then readily solved to yield the jump condition for shocks propagating in an ultra-relativistic gas:

$$\beta_1\beta_2 = \frac{1}{3}. \quad (7)$$

This relation holds for shocks of any strength, provided only that the upstream gas is ultra-relativistic. The only requirement for the existence such of a shock solution is that the upstream flow velocity be larger than the sound speed in the upstream gas, which is $c/\sqrt{3}$ for an ultra-relativistic gas.

Strong Shocks and the Sygne Equation of State

I now consider the case of a *strong shock*, i.e. one in which the thermal energy upstream is negligible with respect to the bulk flow kinetic energy, so that one may neglect the upstream pressure p_1 and write $\varepsilon_1 \approx n_1 mc^2$ in (2) and (3), where m is the mass of individual gas particles, assumed for simplicity to belong

to a single species. For the downstream equation of state, I use that of an ideal gas of arbitrary temperature, as given by Sygne [29]:

$$\varepsilon_2 + p_2 = n_2 mc^2 G\left(\frac{mc^2}{T_2}\right). \quad (8)$$

Here T_2 is the downstream gas temperature, and the function $G(\xi)$ is defined in terms of modified Bessel functions of the first kind, $G(\xi) \equiv K_3(\xi)/K_2(\xi)$, and has the asymptotic expansions:

$$G\left(\frac{mc^2}{T}\right) = 1 + \frac{5}{2} \frac{T}{mc^2} + \mathcal{O}\left(\frac{T}{mc^2}\right)^2, \quad T \ll mc^2, \quad (9)$$

$$G\left(\frac{mc^2}{T}\right) = \frac{4T}{mc^2} + \frac{mc^2}{2T} + \mathcal{O}\left(\frac{mc^2}{T}\right)^3, \quad T \gg mc^2. \quad (10)$$

Using the fact that the gas always obeys the ideal gas law $p = nT$, it is readily seen that these two asymptotes correspond to the familiar equations of state for non-relativistic and ultra-relativistic ideal gases, namely $\varepsilon = nmc^2 + 3p/2$ and $\varepsilon = 3p$, respectively.

With the above assumptions, the shock jump conditions (1–3) may be solved by first using (1) to rewrite (2) and (3) in terms of the normalised quantities

$$\bar{\varepsilon}_2 \equiv \frac{\varepsilon_2}{n_2 mc^2} = G(\xi) - \frac{1}{\xi}, \quad (11)$$

$$\bar{p}_2 \equiv \frac{p_2}{n_2 mc^2} = \frac{1}{\xi}, \quad (12)$$

where the *reciprocal temperature* of the downstream gas has been defined as $\xi \equiv mc^2/T_2$. The two resulting equations may be solved to yield Γ_1 and Γ_2 in terms of ξ [20]:

$$\Gamma_2^2 = \frac{\bar{\varepsilon}_2^2 - 1}{\bar{\varepsilon}_2^2 - \bar{p}_2^2 - 1}, \quad (13)$$

$$\Gamma_1 = (\bar{\varepsilon}_2 + \bar{p}_2)\Gamma_2. \quad (14)$$

If one prefers to use Γ_1 rather than T_2 as the independent variable, the analytical equation (14), substituting the definitions (11–13), may be inverted numerically. The shock velocity ratio β_1/β_2 resulting from (13–14) is shown in Fig. 1 as a function of the upstream four-velocity $\beta_1\Gamma_1$, along with the corresponding result for the ultra-relativistic upstream gas case (7).

Electron–Ion Plasmas: The shock jump conditions derived above, based on the equation of state (8), are strictly speaking only valid for a gas composed of particles of a single mass m , as would be the case for instance in an electron–positron plasma. Equation (8) is readily generalised to a gas composed of species of different masses [20,29], assuming they are in thermal equilibrium. However,

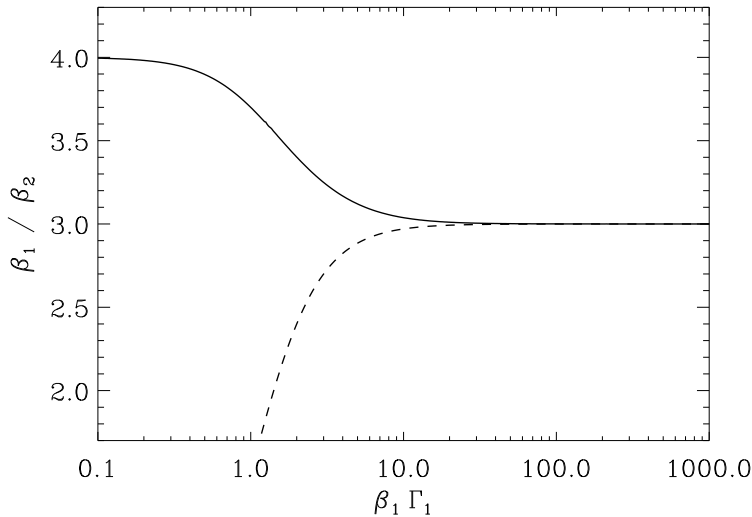


Fig. 1. The shock velocity ratio as a function of the upstream four-velocity, for the two extreme cases of a cold gas upstream obeying the Synge equation of state downstream (*solid line*), and of an ultra-relativistically hot gas upstream (*dashed line*)

simulations of relativistic, perpendicular shocks in electron–ion plasmas [18] show that the species do not in fact achieve thermal equilibrium immediately behind the shock, but instead have distinct temperatures corresponding to the thermalisation of their respective upstream bulk kinetic energy. The strong shock jump condition illustrated in Fig. 1 then also applies in this case, as I now demonstrate.

As remarked in [20], for a strong shock one may derive from the shock jump conditions (1–3) the relation

$$\varepsilon_2 = \Gamma_{\text{rel}} \rho_2 c^2, \quad (15)$$

where ρ_2 is the total downstream rest mass density, and Γ_{rel} the Lorentz factor corresponding to the relative velocity (6). This equation shows that the downstream energy density per unit mass is simply the upstream bulk flow energy of the particles as seen from the downstream frame. If this relation holds separately for each species, as is the case initially in the electron–ion shock simulations mentioned above, one has for each species, using (11):

$$G(\xi) - \frac{1}{\xi} = \Gamma_{\text{rel}}. \quad (16)$$

Thus although the temperatures of the species will in general be different, their normalised (reciprocal) temperatures ξ will be the same, and the shock jump conditions obtained above for a single particle mass will hold in this case also.

Energy exchange between the electrons and the ions does take place downstream of the shock in the above-mentioned simulations, but appears to result

in a power-law tail of the electron energy distribution rather than simple heating, as discussed further in Sect. 4.4. One could envision shock jump conditions taking into account this phenomenon in the downstream equation of state; however, an equally important component of more realistic shock jump conditions is the energy and momentum carried away by the strong electromagnetic precursor emitted by the shock front [16]. As neither of these two phenomena can be predicted quantitatively at present, it seems premature to attempt to obtain more accurate shock jump conditions for electron-ion plasmas than that shown in Fig. 1 for a simple Sygne equation of state.

3 Fermi Acceleration and the Spectral Index

In this section, I first review the basic ideas of the Fermi acceleration mechanism in the context of non-relativistic shocks, then discuss in some detail its application to the opposite extreme of ultra-relativistic shocks and the spectral index resulting in that case, before addressing the more involved intermediate case of moderately relativistic shocks.

3.1 Non-Relativistic Shocks

While the essential concepts of the acceleration mechanism that bears his name date back to Fermi [10], their application to shock acceleration was first proposed in 1977–78 in four independent papers [2,4,9,23]; of these, I will follow most closely below the treatment given by Bell [4].

The acceleration scenario is illustrated schematically in Fig. 2: a high-energy particle, assumed for simplicity to be already relativistic, diffuses through the medium on either side of the shock by scattering on magnetic irregularities. These may be, for instance, Alfvén waves self-consistently excited by the diffusing high-energy particles [5]. Assuming the local Alfvén velocity is much smaller than the shock velocity, to lowest order the magnetic scattering centres may be considered at rest with respect to the fluid, so that the scattering events do not change the particle energy in the local fluid rest frame.

Consider, then, a particle diffusing upstream or downstream while preserving its energy in the corresponding rest frame. A particle initially having energy E_i in the upstream medium will eventually cross the shock, its velocity upon crossing making an angle $\theta_{\rightarrow d}$ with the shock normal (see Fig. 2). Its energy measured in the downstream frame, E'_i , will then be given by the appropriate Lorentz transformation, and preserved while the particle is downstream. If it re-crosses the shock into the upstream medium, this time at an angle $\theta'_{\rightarrow u}$, its final energy upstream, E_f , will be given by the combination of the two Lorentz transformations:

$$\frac{E_f}{E_i} = \Gamma_{\text{rel}}^2 (1 - \beta_{\text{rel}} \mu_{\rightarrow d}) (1 + \beta_{\text{rel}} \mu'_{\rightarrow u}), \quad (17)$$

where β_{rel} and Γ_{rel} are the relative velocity of the upstream and downstream media and the corresponding Lorentz factor, and I have introduced the notation μ for $\cos \theta$. Here and in what follows primed and unprimed quantities are

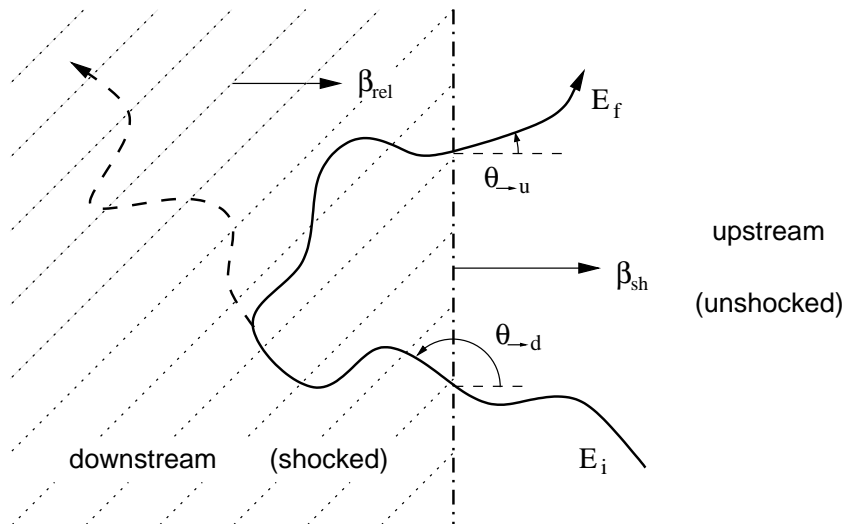


Fig. 2. Schematic representation of one cycle of shock acceleration: a shock propagates with velocity β_{sh} into the undisturbed (upstream) medium to the right; the velocity of the shocked (downstream) medium relative to the upstream one is β_{rel} . A relativistic particle diffuses through the media on both sides of the shock, crossing and re-crossing it at incidence angles $\theta_{\rightarrow\text{d}}$ and $\theta_{\rightarrow\text{u}}$, with initial and final energies E_i and E_f

respectively measured in the downstream and upstream rest frames. The only approximation made in deriving (17) is that that the particle is highly relativistic, so that the rest mass contribution to its energy may be neglected.

For non-relativistic shocks, $\beta_{\text{rel}} \ll 1$, the angular distribution of these scattered particles crossing the shock may be approximated as isotropic, so that the flux-weighted averages of the direction angle cosines, over the relevant ranges $-\pi/2 \leq \theta_{\rightarrow\text{d}} \lesssim 0$ and $0 \lesssim \theta'_{\rightarrow\text{u}} \leq \pi/2$, are respectively $\langle \mu_{\rightarrow\text{d}} \rangle \approx -2/3$ and $\langle \mu'_{\rightarrow\text{u}} \rangle \approx 2/3$. The average energy gain (17) per shock crossing cycle then reduces to

$$\left\langle \frac{E_f}{E_i} \right\rangle \approx 1 + \beta_{\text{rel}} (\langle \mu'_{\rightarrow\text{u}} \rangle - \langle \mu_{\rightarrow\text{d}} \rangle) \approx 1 + \frac{4}{3} \beta_{\text{rel}}. \quad (18)$$

Fermi shock acceleration is sometimes referred to as the *Fermi I* mechanism because this energy gain is of first order in the velocity β_{rel} .

While a particle upstream will always eventually cross the shock, at least in the simple case considered here of an infinite, plane-parallel shock, once downstream the particle has a certain probability of being advected away and never re-crossing the shock. This *escape probability* may be evaluated from the ratio of the average fluxes of particles escaping far downstream and crossing the shock. For a downstream flow velocity β_2 , again assuming isotropy of the relativistic particle distribution, it is given by $P_{\text{esc}} = 4\beta_2$.

The combination of the energy gain factor (18) and escape probability P_{esc} leads to a power-law spectrum in the accelerated particle energy, with a spectral index depending solely on the shock jump conditions:

$$\frac{dN}{dE} \propto E^{-(r+2)/(r-1)}, \quad (19)$$

where $r \equiv \beta_1/\beta_2$ is the shock *velocity ratio*. For a strong, non-relativistic shock in a monatomic gas, $r = 4$, leading to a spectral index $(r+2)/(r-1) = 2$ for the accelerated particles. In reality, spectral indices somewhat steeper than this value are often observed; this difference may be due to the pressure of the accelerated particles modifying the shock structure (e.g. [7] and references therein).

3.2 Ultra-Relativistic Shocks

I now turn my attention to ultra-relativistic shocks, i.e. those for which $\Gamma_{\text{sh}} \gg 1$ so that the shock jump conditions derived in Sect. 2.2 apply.

Energy Gain and Upstream Particle Dynamics

For a downstream particle to cross the shock into the upstream medium, it must have $1 \geq \mu'_{\rightarrow\text{u}} > \beta'_{\text{sh}} = \frac{1}{3}$, so that the factor $(1 + \beta_{\text{rel}}\mu'_{\rightarrow\text{u}})$ in (17) is always of order unity. If $\mu_{\rightarrow\text{d}}$ is approximately isotropically distributed, as might be the case for a population of relativistic particles already present in the undisturbed upstream medium, the factor $(1 - \beta_{\text{rel}}\mu_{\rightarrow\text{d}})$ is in general also of order unity. Thus in the first shock crossing cycle, a large *initial boost* in energy can be achieved, $E_i/E_f \sim \Gamma_{\text{rel}}^2$ as envisioned in [30].

For all subsequent shock crossing cycles, however, the distribution of $\mu_{\rightarrow\text{d}}$ will be highly anisotropic; this is an essential difference between non-relativistic and relativistic Fermi shock acceleration [22,27]. For an ultra-relativistic particle with Lorentz factor $\gamma \gg \Gamma_{\text{sh}}$, the kinematic condition to cross the shock into the upstream medium reduces to $\theta_{\rightarrow\text{u}} < 1/\Gamma_{\text{sh}}$. As shown in [13], for realistic deflection processes upstream the particle cannot be deflected very far beyond this ‘loss cone’ before the shock overtakes it, so that $\theta_{\rightarrow\text{d}} \sim 1/\Gamma_{\text{sh}}$ as well. In this case the energy gain factor reduces to

$$\frac{E'_f}{E'_i} \approx \frac{2 + (\Gamma_{\text{sh}}\theta_{\rightarrow\text{d}})^2}{2 + (\Gamma_{\text{sh}}\theta_{\rightarrow\text{u}})^2} \approx \frac{1 + \mu'_{\rightarrow\text{u}}}{1 + \mu'_{\rightarrow\text{d}}}, \quad (20)$$

where the shock crossing cycle is now considered from downstream to upstream and back.

The range of possible energy gain factors can be assessed by considering two opposite extremes for the upstream particle dynamics: deflection by a regular magnetic field and scattering by small-scale magnetic fluctuations. In terms of the correlation length ℓ of the magnetic field, these two regimes respectively correspond to $R_L/\Gamma_{\text{sh}} \ll \ell$ and $R_L/\Gamma_{\text{sh}} \gg \ell$, where R_L is the Larmor radius

of the particle. For regular deflection, it can be shown that for ingress angles $0 \leq \Gamma_{\text{sh}}\theta_{\rightarrow\text{u}} < 1$, the egress angle satisfies

$$1 < \Gamma_{\text{sh}}\theta_{\rightarrow\text{d}} \leq 2 \quad \iff \quad \frac{1}{3} > \mu'_{\rightarrow\text{d}} \geq -\frac{1}{3}, \quad (21)$$

while for direction-angle scattering, the direction angle at the average shock recrossing time satisfies

$$\langle \theta_{\rightarrow\text{d}}^2 \rangle \approx \frac{2}{\Gamma_{\text{sh}}^2} - \theta_{\rightarrow\text{u}}^2. \quad (22)$$

In both cases, it may be seen that the typical energy gain $\Delta E' \equiv E'_f - E'_i$ is thus of the order of E'_i itself [13].

Numerical Calculation of the Angular Distribution

As was seen in the case of non-relativistic shock acceleration, the power-law index of the accelerated particle distribution depends on the average energy gain per shock crossing and the escape probability. For relativistic shocks, both of these are strongly dependent on the angular distribution of particles crossing the shock, which as suggested in the previous section is in general highly anisotropic. Thus the quasi-isotropic approximations used in the non-relativistic case do not apply here, and the distribution of the shock crossing angles $\mu_{\rightarrow\text{u}}$ and $\mu_{\rightarrow\text{d}}$ has been evaluated numerically.

For simplicity, I will focus in this section on the case where both the upstream and downstream particle dynamics are dominated by scattering of the particle momentum direction. In other words, it is assumed that magnetic fluctuations dominate over the regular magnetic field in determining the particle transport, at least along the shock normal direction which is of interest here. This is a highly plausible assumption downstream, where shock-generated turbulence is likely to give rise to disordered magnetic fields significantly stronger than the shock-compressed upstream field, as is assumed in relativistic fireball models of gamma-ray bursts and their afterglows (see Sari & Galama, this volume).

One method of computing the accelerated particle distribution is through numerical simulations, and I illustrate below the results of such a calculation, after summarising the algorithm: since the nature of the particle transport upstream and downstream is by assumption independent of particle energy, it is computationally more efficient to decouple the dynamical problem from the energy gains. A numerical approximation to the function $f_{\text{d}}(\mu'_{\rightarrow\text{u}}; \mu'_{\rightarrow\text{d}})$, the distribution of downstream egress angles $\mu'_{\rightarrow\text{u}}$ for a given ingress angle, is thus first constructed by Monte-Carlo simulation of the downstream scattering process for a grid of $\mu'_{\rightarrow\text{d}}$ values. The upstream dynamics are represented by a similarly obtained upstream egress angle distribution $f_{\text{u}}(\mu_{\rightarrow\text{d}}; \mu_{\rightarrow\text{u}})$, and both distributions, along with the energy gain formula (20), are subsequently used in a Monte-Carlo calculation of the steady-state flux of accelerated particles crossing the shock.

The results of such a calculation were summarised in [14]. The influence of the highly anisotropic injected particle distribution was seen to disappear at

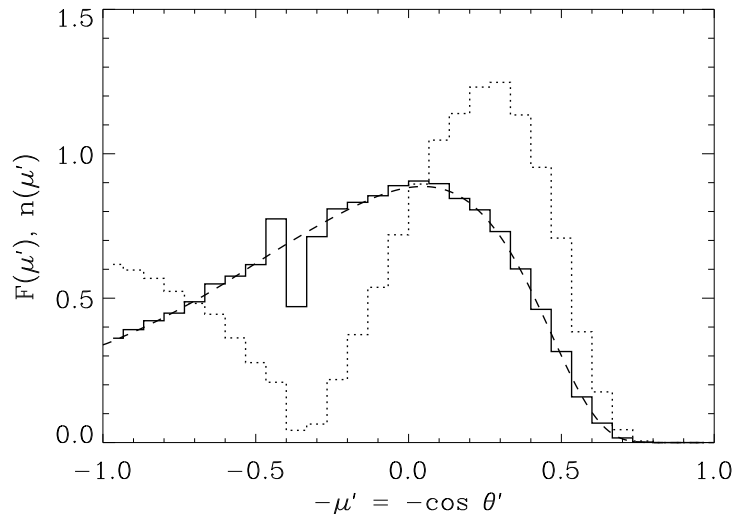


Fig. 3. Asymptotic downstream angular distribution of the particles crossing the shock, showing both the flux $F(\mu')$ (dotted line) and density $n(\mu')$ (solid line) obtained by Monte-Carlo simulations, along with the density obtained by the eigenfunction method (dashed line). All distributions are normalised to unity

a little more than a decade above the downstream injection energy, at which point the self-consistent angular distribution was established with a power-law in energy, $F(E', \mu') \propto F(\mu')E'^{-p}$. Here F represents the steady-state flux of accelerated particles crossing the shock, per unit energy E' and direction angle cosine μ' . The asymptotic angular distribution obtained with this simulation method is displayed in Fig. 3, which shows both $F(\mu')$ and the corresponding density distribution, $n(\mu') \propto F(\mu')/(\mu' - \beta'_{\text{sh}})$. The latter is compared with the distribution obtained with the very different semi-analytical eigenfunction method of Kirk et al. [21], showing excellent agreement between the two methods.

Spectral Index and Comparison with Observations

In the case considered above of isotropic scattering upstream and downstream of the shock due to a strongly turbulent magnetic field, a value of the spectral index $p = 2.23 \pm 0.01$ is found by both Monte-Carlo simulations [1,14] and the semi-analytical eigenfunction method [21]. For the opposite extreme in upstream dynamics of deflection by a regular magnetic field (see above), still assuming isotropic scattering downstream, Monte-Carlo simulations yield $p = 2.30$ [1]. With particle transport including both a regular field and magnetic fluctuations, Bednarz and Ostrowski [3] obtained in Monte-Carlo simulations values of $p \approx 2.2$ in the limit $\Gamma_{\text{sh}} \gg 1$. A spectral index in the range $p = 2.2$ – 2.3 is thus a general feature of Fermi acceleration at (weakly magnetised) ultra-relativistic shocks, at least in the test-particle approximation used in all the above studies.

Spectral index values deduced from observations of astrophysical systems thought to involve ultra-relativistic shocks are consistent with these theoretical expectations. Early modelling of gamma-ray burst afterglow observations suggested $p = 2.3 \pm 0.1$ [32], and detailed analysis of the GRB 970508 afterglow spectrum yielded $p = 2.2$ [12]. While an equally detailed multi-wavelength spectral analysis has not been published for other afterglows, a value of $p \approx 2.2$ seems compatible with most [11]. In Crab-like supernova remnants, the inferred spectral indices are similar: the best-fit model for the Crab Nebula spectrum corresponds to p in the range 2.2–2.3 [19]. The very good agreement between theory and observation is all the more remarkable given that in non-relativistic shocks, as mentioned above, the observed particle spectra often differ from the predictions of the simple test-particle theory.

3.3 Moderately Relativistic Shocks

For moderately relativistic shocks, the self-consistent shock crossing angle distribution and the spectral index depend on the shock jump conditions assumed, as well as the shock Lorentz factor Γ_{sh} , which together determine the shock velocity ratio. Figure 4 shows, for illustration, the spectral indices obtained with the eigenfunction method of Kirk et al. [21] in the two extreme cases considered in Sect. 2.3, namely that where the upstream gas is ‘cold’ so that the shock is strong, and that where it is ultra-relativistically hot.

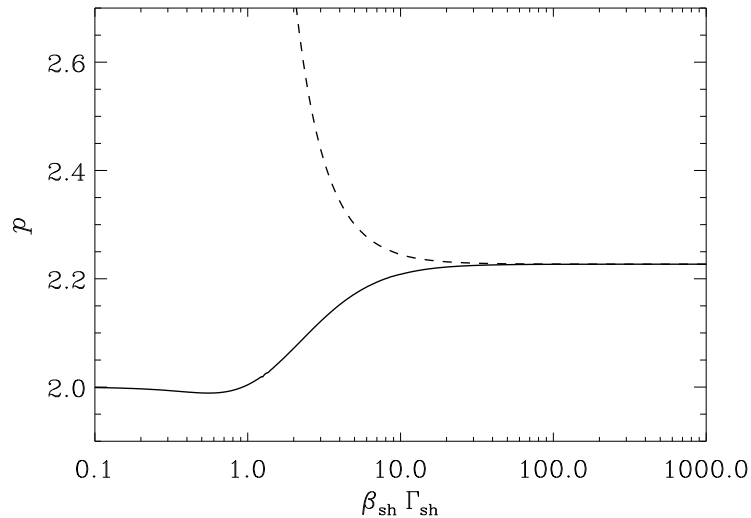


Fig. 4. Spectral index of the Fermi-accelerated particle distribution as a function of the shock four-velocity, for the two extreme cases shown in Fig. 1, namely a cold upstream gas (*solid line*) and an ultra-relativistically hot one (*dashed line*)

It is readily seen that while for high Lorentz factors ($\Gamma_{\text{sh}} \gtrsim 10$) the values obtained rapidly converge to the ultra-relativistic case, for lower shock Lorentz factors the different shock jump conditions yield very different spectral indices. In particular, for moderately relativistic shocks in a relativistically hot gas, which might be relevant to internal shocks in gamma-ray bursts, the spectral indices obtained can be significantly steeper than in the ultra-relativistic case. For strong shocks, on the other hand, the spectral index goes smoothly from the ultra-relativistic value of $p = 2.23$ to the non-relativistic one of $p = 2$ as the shock Lorentz factor decreases.

The above results apply to unmagnetised shocks and isotropic direction-angle diffusion both upstream and downstream. A non-negligible magnetisation parameter (4) lowers the strong shock velocity ratio, leading to steeper values of the spectral index than in the corresponding unmagnetised case [21]. Anisotropic diffusion in direction angle can have the opposite effect: calculations for the extreme case where the magnetic fluctuations are concentrated in the plane of the shock yield somewhat flatter spectra than the isotropic case, but by less than 0.1 in the spectral index p [21]. Anisotropic *pitch-angle* diffusion has been simulated by Bednarz and Ostrowski [3], who obtained steeper spectral indices for weak scattering, the regime considered above corresponding to the limit of strong scattering.

4 Maximum and Minimum Particle Energies

I now turn to the question of the range in particle energies over which the spectrum derived above applies. I first discuss the acceleration time scale for the Fermi mechanism, then use it to derive the maximum energy attainable by this process at a relativistic blast wave, and consider an alternative scenario involving the initial boost which can reach higher energies. I also discuss the minimum energy for Fermi acceleration, and the need for a distinct electron pre-acceleration mechanism in electron-ion shocks.

4.1 Acceleration Time Scale

The acceleration time scale t_{acc} is defined as the time needed for the particle energy to increase by an amount of order itself. Since, as seen in Sect. 3.2, this typically occurs every shock crossing cycle, t_{acc} is roughly the cycle time, which is the sum of the upstream and downstream *residence times* t_{up} and t_{dn} . In the case of deflection by a uniform magnetic field upstream, the former is of order

$$t_{\text{up}} \sim \frac{1}{\Gamma_{\text{sh}} \omega_{c\perp}} \equiv \frac{E}{q \Gamma_{\text{sh}} B_{1\perp} c}, \quad (23)$$

where q and ω_c are the particle's charge and cyclotron frequency. The downstream residence time depends on the downstream scattering process; assuming Bohm diffusion, it is roughly the downstream gyrotime,

$$t'_{\text{dn}} \sim \frac{1}{\omega'_c} \equiv \frac{E'}{q B'_2 c}, \quad (24)$$

where primed quantities are measured in the downstream rest frame, as before. If the downstream magnetic field is simply the compressed value resulting from the (weakly magnetised) ultra-relativistic shock jump conditions, $B'_2 \approx B'_{2\perp} \approx \sqrt{8}\Gamma_{\text{sh}}B_{1\perp}$, it can be shown that $t_{\text{dn}} \sim t_{\text{up}}$ [13].

Turbulence downstream may amplify the magnetic field B'_2 by a significant factor above the shock-compressed value, thereby reducing the downstream residence time by the same factor; assuming the field reaches equipartition with the thermal pressure downstream, this factor will be of order c/v_A , where v_A is the upstream Alfvén speed. On the other hand, in the case of scattering by small-scale magnetic fluctuations, the upstream residence time is increased from the value (23) by a factor of order $R_L/(\Gamma_{\text{sh}}\ell)$, where ℓ , as before, is the correlation length of the magnetic field [13]. Thus the value of t_{up} given in (23) is a lower limit to t_{acc} in all cases of interest.

4.2 Relativistic Blast Waves and Ultra-High-Energy Cosmic Rays

An immediate application of the above considerations is to the maximum energy attainable by Fermi acceleration at the relativistic blast waves occurring in fireball models of gamma-ray bursts; I thus first review some basic properties of these models. After an acceleration stage, an initially radiation-dominated fireball enters a relativistic ‘free expansion’ phase, in which a blast wave is driven into the surrounding medium with the approximately constant Lorentz factor $\Gamma_{\text{sh}} \approx \sqrt{2}\eta$, where $\eta \equiv \mathcal{E}/(Mc^2)$, M being the baryonic mass in which the fireball energy \mathcal{E} is initially deposited [24,28]. This is followed by an adiabatic deceleration phase in which the blast wave Lorentz factor decreases with radius R_{sh} as $\Gamma_{\text{sh}} \propto R_{\text{sh}}^{-3/2}$ [8]. The transition between these two phases occurs around the deceleration radius R_{dec} , given by

$$R_{\text{dec}} \approx \left(\frac{3}{4\pi} \frac{\mathcal{E}}{\eta^2 \varepsilon_1} \right), \quad (25)$$

where $\varepsilon_1 \approx n_1 mc^2$ is the energy density of the surrounding material.

In the absence of energy loss processes, the maximum particle energy attainable by Fermi acceleration is set by the requirement that t_{acc} be shorter than the age of the system, which for a relativistic blast wave is simply R_{sh}/c . Using (23) for t_{acc} , the resulting maximum energy at a given blast wave radius R_{sh} is

$$E_{\text{max}} \approx qB_1\Gamma_{\text{sh}}R_{\text{sh}}. \quad (26)$$

Note that this is larger by a factor Γ_{sh} than a commonly used estimate resulting from a simple geometrical comparison of the particle Larmor radius with R_{sh} [17]. This is due to features specific to particle acceleration at a relativistic blast wave, in particular the fact that an accelerated particle typically executes only a fraction $\sim 1/\Gamma_{\text{sh}}$ of a Larmor orbit upstream before recrossing the shock.

The evolution of the product $\Gamma_{\text{sh}}R_{\text{sh}}$ with R_{sh} implies that the highest E_{max} is reached at the deceleration radius, $R_{\text{sh}} \approx R_{\text{dec}}$. It has the numerical value

$$E_{\text{max}} \approx 5 \times 10^{15} ZB_{-6} \left(\frac{\mathcal{E}_{52}\eta_3}{n_0} \right)^{1/3} \text{ eV}, \quad (27)$$

for particles of charge $q = Ze$, where B_{-6} is the upstream magnetic field, \mathcal{E}_{52} the (isotropic) fireball energy, η_3 the initial Lorentz factor and n_0 the upstream density, respectively in units of microgauss, 10^{52} erg, 10^3 and cm^{-3} , these normalising values being those appropriate for a GRB fireball expanding into a generic interstellar medium [13].

Equation (27) rules out the production of ultra-high-energy cosmic rays (UHECRs), with energies up to $\sim 10^{20}$ eV, at the *unmodified, external* blast waves of relativistic fireballs. Scenarios which postulate a GRB origin for UHECRs [25,30,31] must thus invoke some other site or mechanism to reach the required particle energies. The idea most often put forward is that UHECRs are accelerated at internal shocks, where substantially higher magnetic fields, close to equipartition, could be present both upstream and downstream and allow the Fermi mechanism to reach UHECR energies. However, the particle spectrum in this case would likely be steeper, as argued above, reducing the efficiency of UHECR production. Moreover, the important issue of the escape of these particles from the interior of the fireball to the surrounding medium remains to be investigated, as they could suffer significant adiabatic losses due to the fireball expansion before escaping.

Another possibility for acceleration at the blast wave is that the upstream magnetic field might be amplified by a large factor above its undisturbed value due to instabilities driven by the accelerated particles themselves, as was recently proposed in the context of supernova remnants by Bell and Lucek [6]. It is unclear, however, how far such instabilities would have time to develop in the relativistic context, given the comparatively short time before the modified upstream medium is overtaken by the shock.

4.3 Fireballs in Pulsar Wind Bubbles

An alternative scenario for UHECR acceleration is based on the observation that the *initial boost* examined in Sect. 3.2 can circumvent the age limit (27), as it involves only a downstream half-cycle. The maximum energy is then set only by the requirement that the downstream residence time t_{dn} be less than the age of the system. If one assumes that the downstream magnetic field is turbulently amplified close to equipartition values, energies of order 10^{20} eV or more can be reached, provided that a population of relativistic particles with sufficient initial energy to be boosted into this range is present upstream [13].

Galactic cosmic rays with appropriate energies are present in the interstellar medium, but constitute only a small fraction of the upstream energy density, so that only a correspondingly small fraction of the fireball energy could go to boost these to UHECR energies. However, a situation where the surrounding medium consists almost exclusively of relativistic particles of the required energy occurs naturally in the context of neutron star binary merger events: the close binary pulsar systems observed in our Galaxy, which are the progenitors of these merger events, all contain millisecond pulsars with characteristic spindown times of order 10^8 yr, while their spiral-in times due to gravitational radiation are of order 3×10^7 yr [26]. These pulsars thus fill the surrounding space with relativistic

particles over the lifetime of the binary system, forming a large pulsar wind bubble in the interstellar medium.

While the majority constituents of these pulsar wind bubbles will likely be electron-positron pairs, pulsar winds also seem to contain ions [15,18]. Scaling this ion component to millisecond pulsar parameters, one can show that it yields ions with energies $\sim 10^{14}$ eV, sufficient to be boosted to UHECR energies provided $\Gamma_{\text{sh}} \gtrsim 10^3$. This process is now highly efficient: a large fraction of the fireball energy can go to boost these ions to UHECR energies. Moreover, for typical parameters the blast wave will decelerate within the pulsar wind bubble, resulting in a power-law spectrum of boosted ions,

$$\frac{dN}{dE} \propto E^{-2}, \quad (28)$$

with a lower bound of $\sim 3 \times 10^{18}$ eV, compatible with the inferred UHECR source spectrum [13]. This scenario thus naturally provides for the acceleration of UHECRs into the required energy range, with the required spectrum, and with high efficiency.

4.4 Minimum Energy and Electron Pre-Acceleration

Returning now to the Fermi acceleration mechanism proper, it has as one of its requirements that accelerated particles see the shock as a sharp discontinuity, as its treatment in Sect. 3 makes clear. For this to be the case, the particle Larmor radius must be larger than the shock thickness, which is in turn roughly given by the downstream thermal ion Larmor radius. Ions can thus undergo Fermi acceleration when they have reached a few times their downstream thermal energy, but electrons in electron-ion shocks must first reach a minimum energy

$$E'_{\text{min}} \sim \Gamma_{\text{rel}} m_i c^2, \quad (29)$$

where m_i is the ion mass, before participating in the Fermi mechanism and acquiring its characteristic spectral index.

Unless one assumes that these objects involve solely electron-positron shocks, the presence of synchrotron-emitting, Fermi-accelerated electrons in GRB afterglows and Crab-like supernova remnants thus requires an electron pre-acceleration mechanism. This mechanism must bring the electron energy from that resulting from randomisation of the bulk upstream energy, which as seen in Sect. 2.3 is $E'_{\text{th}} = \Gamma_{\text{rel}} m_e c^2$, to E'_{min} , a factor of the mass ratio m_i/m_e higher. An acceleration process operating over precisely this energy range is the resonant ion cyclotron wave absorption mechanism discovered by Hoshino et al. [18] in numerical simulations of highly relativistic, electron-positron-ion shocks.

This resonant ion cyclotron acceleration mechanism typically yields harder power-law spectra than those resulting from Fermi acceleration: the spectral indices p obtained from the simulations are generally less than 2, and a value as low as $p = 1$ is predicted in a quasi-linear, steady-state approximation [18]. The resulting picture for the accelerated electron (and positron) spectrum in

an ultra-relativistic shock containing ions is thus of a relatively hard power-law spectrum at low energies, steepening to the $p \approx 2.2$ spectrum characteristic of Fermi acceleration at a break energy given by (29). This might explain the flat radio spectral indices of Crab-like supernova remnants, as well as the two breaks in the Crab Nebula spectrum between radio and X-ray frequencies, only one of which can be attributed to synchrotron cooling.

5 Summary

The shock velocity ratio r across a relativistic shock is in general a function of the assumed upstream temperature as well as the shock Lorentz factor Γ_{sh} , but it rapidly tends to the ultra-relativistic limit $r = 3$ for $\Gamma_{\text{sh}} \gtrsim 10$. The ultra-relativistic Fermi acceleration regime then mirrors some of the simplicity of the non-relativistic, strong shock regime, this asymptotic shock velocity ratio corresponding to an asymptotic power-law index of the accelerated particle distribution. For the specific case of isotropic direction-angle scattering on both sides of the shock, this spectral index is $p = 2.23 \pm 0.01$; more generally, a value of p in the range 2.2–2.3 is found under a variety of particle transport assumptions. These values are consistent with the observed spectra of sources thought to contain ultra-relativistic shocks, such as gamma-ray burst afterglows and Crab-like supernova remnants. For moderately relativistic shocks, the spectral index depends on the shock jump conditions as well as Γ_{sh} ; in particular, shocks in a relativistic gas typically yield steeper spectral indices than the above ultra-relativistic values.

The maximum energy E_{max} of the Fermi-accelerated particle distribution is determined by the acceleration time, which is in general set by the upstream residence time. For acceleration at the unmodified, external blast wave of relativistic fireballs, this yields $E_{\text{max}} \sim 10^{16}$ eV for typical parameters of the surrounding interstellar medium, ruling out the production of ultra-high-energy cosmic rays in this context. If neutron star binary merger events give rise to relativistic blast waves with $\Gamma_{\text{sh}} \gtrsim 10^3$, these can provide an alternative scenario for UHECR production: ions accelerated in the pulsar wind present before the merger can be boosted to energies $\gtrsim 10^{20}$ eV by the blast wave with high efficiency; deceleration of the blast wave in the pulsar wind bubble yields a spectral index $p = 2$ and a typical lower cutoff around 3×10^{18} eV. There is also a minimum energy for Fermi acceleration, set by the requirement that the shock thickness be small relative to the particle Larmor radius. In electron–ion shocks, this requires a distinct pre-acceleration mechanism for the electrons, which could be the resonant ion cyclotron wave acceleration mechanism of Hoshino et al. [18].

Acknowledgements

I gratefully acknowledge support from the Italian Ministry of University and Research through grant Cofin–99–02–02, and the Netherlands Organisation for Scientific Research (NWO) through GBE/MPR grant 614–21–008.

References

1. A. Achterberg, Y.A. Gallant, J.G. Kirk, A.W. Guthmann: M.N.R.A.S, submitted (2001)
2. W.I. Axford, E. Leer, G. Skadron: In: *15th International Cosmic Ray Conference, at Plovdiv, Bulgaria, August 13–26, 1977. Conference Papers*, Vol. 11, p. 132 (Bulgarian Academy of Sciences, Sofia 1978)
3. J. Bednarz, M. Ostrowski: Phys. Rev. Lett. **80**, 3911 (1998)
4. A.R. Bell: M.N.R.A.S. **182**, 147 (1978)
5. A.R. Bell: M.N.R.A.S. **182**, 443 (1978)
6. A.R. Bell, S.G. Lucek: M.N.R.A.S. **321**, 433 (2001)
7. E.G. Berezhko, D.C. Ellison: Ap. J. **526**, 385 (1999)
8. R.D. Blandford, C.F. McKee: Phys. Fluids **19**, 1130 (1976)
9. R.D. Blandford, J.P. Ostriker: Ap. J. **221**, L29 (1978)
10. E. Fermi: Phys. Rev. **75**, 1169 (1949)
11. D.A. Frail, T.J. Galama: personal communication (2000)
12. T.J. Galama, R.A.M.J. Wijers, M. Bremer, P.J. Groot, R.G. Strom, A.G. de Bruyn, C. Kouveliotou, C.R. Robinson, J. van Paradijs: Ap. J. **500**, L101 (1998)
13. Y.A. Gallant, A. Achterberg: M.N.R.A.S. **305**, L6 (1999)
14. Y.A. Gallant, A. Achterberg, J.G. Kirk, A.W. Guthmann: In: *5th Huntsville Gamma-Ray Burst Burst Symposium*, ed. by R.M. Kippen, R.S. Mallozzi, G.J. Fishman, p. 524 (AIP, New York 2000)
15. Y.A. Gallant, J. Arons: Ap. J. **435**, 230 (1994)
16. Y.A. Gallant, M. Hoshino, A.B. Langdon, J. Arons, C.E. Max: Ap. J. **391**, 73 (1992)
17. A.M. Hillas: Ann. Rev. Astron. Astrophys. **22**, 425 (1984)
18. M. Hoshino, J. Arons, Y.A. Gallant, A.B. Langdon: Ap. J. **390**, 454 (1992)
19. C.F. Kennel, F. Coroniti: Ap. J. **283**, 710 (1984)
20. J.G. Kirk, P. Duffy: J. Phys. G **25**, R163 (1999)
21. J.G. Kirk, A.W. Guthmann, Y.A. Gallant, A. Achterberg: Ap. J. **542**, 235 (2000)
22. J.G. Kirk, P. Schneider: Ap. J. **315**, 425 (1987)
23. G.F. Krymskii: Sov. Phys. Dokl. **22**, 327 (1977)
24. P. Mészáros, P. Laguna, M.J. Rees: Ap. J. **415**, 181 (1993)
25. M. Milgrom, V. Usov: Ap. J. **449**, L37 (1995)
26. R. Narayan, B. Paczyński, T. Piran: Ap. J. **395**, L83 (1992)
27. J.A. Peacock: M.N.R.A.S. **196**, 135 (1981)
28. T. Piran, A. Shemi, R. Narayan: M.N.R.A.S. **263**, 861 (1993)
29. J.L. Synge: *The Relativistic Gas* (North-Holland, Amsterdam 1957)
30. M. Vietri: Ap. J. **453**, 883 (1995)
31. E. Waxman: Phys. Rev. Lett. **75**, 386 (1995)
32. E. Waxman: Ap. J. **485**, L5 (1997)